Materialia 2 (2018) 190–195

Contents lists available at ScienceDirect

Materialia

journal homepage: www.elsevier.com/locate/mtla

Phase transformations in the W–Cr system at the nanoscale

J. Sebastian Riano[a], Andrea M. Hodge[a,b,*]

[a] Department of Chemical Engineering and Materials Science, University of Southern California, 3650 McClintock Ave., Los Angeles, CA 90089, USA
[b] Department of Aerospace and Mechanical Engineering, University of Southern California, 854 Downey Way, Los Angeles, CA 90089, USA

ARTICLE INFO

Keywords:
Phase transformations
Multilayers
Diffusion
Diffusion zone
W_3Cr

ABSTRACT

In order to enhance the thermal stability of nanomaterials, it is important to understand phase transformations at the nanoscale in high detail. In this study, the phase transformations occurring in the nanocrystalline W–Cr system were investigated using nanometallic multilayers to shift the kinetics of nucleation and to increase the diffusivities of W and Cr. The initial metastable state of the multilayers was tailored to favor the formation of solutions rich in W. In addition, the higher diffusivities in the system made it possible to observe the nucleation of the W_3Cr intermetallic at 1000 °C, a temperature lower than that reported in previous studies. In this manuscript, the use of nanometallic multilayers is proposed as an approach to modify the thermal evolution of a nanocrystalline systems and study phase transformations at the nanoscale.

1. Introduction

Nanocrystalline materials have interesting mechanical, electrical, magnetic and optical properties due to their high density of interfaces [1]. However, their application is limited due to their low thermal stability caused by the excess energy at the grain boundaries, which is the driving force for microstructural and phase transformations leading to grain growth [2–4]. Thus, in order to improve the thermal stability of nanomaterials it is necessary to understand both microstructural and phase transformations that occur during annealing of nanoscale materials.

Several authors have successfully studied microstructural transformations such as recrystallization and grain growth at the nanoscale with the objective of developing kinetic expressions that relate internal parameters of the system with temperature and time [5–7]. However, the study of nanoscale phase transformations has been limited by the lack of systems that allow for control over the kinetics of the transformation [8,9]. In addition, previous studies were mainly concerned with the effect of stresses, surface energy, and phase stability, and did not focus on shifting the kinetics of phase formation [10–14].

In this study we develop a systematic approach to study phase transformations using nanometallic multilayers (NMMs) with sufficiently thin layers to enhance the diffusivity of the species in the system, which result in increased rates for the nucleation of new phases [15]. NMMs are nanostructured materials comprised of alternating layers of different compositions that have been used to enhance the mechanical properties and to study thermal processes in nanomaterials [16]. For example, Nb–Al, Co–Al, Ni–Al, Ti–Al, Cu–Ta, and Ti–Ta metallic multilayers have been used to study amorphization reactions and polymorphic transformations [17-19]. However, there is limited research on phase transformations using NMMs with layers thinner than 10 nm.

NMMs can be tailored to control the local composition and the density of interphases, both of which are variables that can be tuned to promote phase transformations during annealing [17]. Heat-treatment of NMMs result in the development of diffusion zones that level out the composition profile between the alternating layers, where new stable and metastable phases form and compete depending on their diffusivity, energy of formation, and surface energy [20]. The phase formation process typically occurs in two stages, nucleation and growth [17]. During nucleation several embryos form and begin to grow until a critical radius is reached, while during the growth stage, atoms move across interfaces as the grain boundaries migrate [15,20]. Considering that nucleation is a stochastic process, the probability of nuclei formation in the diffusion zone could be enhanced by increasing the interphase area, which is possible by decreasing the individual layers thickness [21]. In addition, for the nucleation of new phases to occur, the multilayered structure should be retained while the diffusion zone grows. This condition is satisfied in binary systems with a tendency for nanograin stability, which can be selected using thermal stability maps as a guide [22–25]. For example, in the maps proposed by Murdoch and Schuh, binary alloys are classified as stable, metastable, and unstable based on their enthalpies of mixing and segregation [26]. Using these maps, the W–Cr system, with W as the solvent, was selected to investigate interfacial phase transformations at the nanoscale. In general, the W–Cr phase diagram shows that depending on the composition, W and Cr can form the intermetallic compound

* Corresponding author at: Department of Chemical Engineering and Materials Science, University of Southern California, 3650 McClintock Ave., Los Angeles, CA 90089, USA.
E-mail address: ahodge@usc.edu (A.M. Hodge).

https://doi.org/10.1016/j.mtla.2018.07.021
Received 18 May 2018; Received in revised form 30 July 2018; Accepted 31 July 2018
Available online 6 August 2018

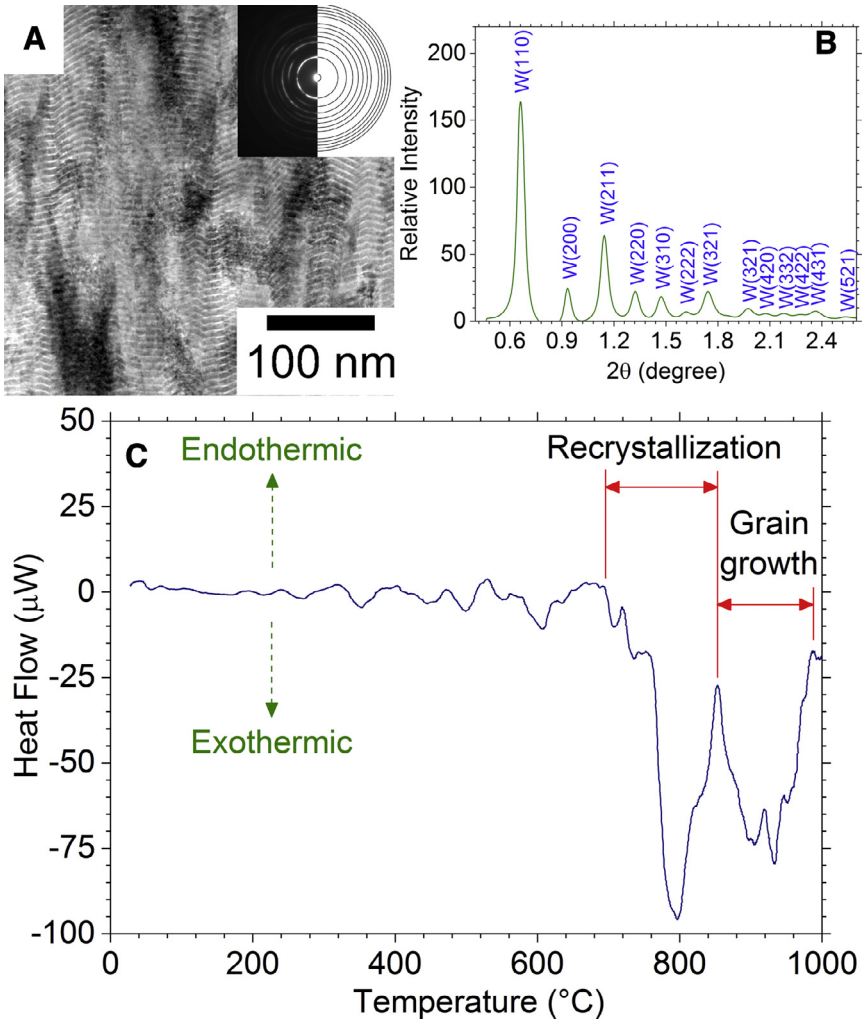

Fig. 1. (a) Cross-sectional bright field STEM and (b) integrated radial intensity profile of as-sputtered W-Cr nanometallic multilayer. Note that only α-Tungsten peaks are observed, indicating that the β-Tungsten phase is not present in the sample. (c) Differential scanning calorimetry scan of the W–Cr nanometallic multilayers from 20 °C to 1000 °C showing that recrystallization and grain growth occur between 690 °C and 990 °C.

W_3Cr or BCC solid solutions which coexist in equilibrium below a miscibility gap (critical temperature of 1677 °C). The W_3Cr intermetallic, with a composition of 25 atomic percent (at%) Cr, has been observed as a tetragonal phase in diffusion couples held at 1350 °C [27]. However, due to the low diffusivities of W and Cr, the W_3Cr phase is unlikely to be observed [28].

Previous studies on the W–Cr system have focused on the possibility of thermodynamically stabilizing W through the segregation of Cr to the grain boundaries [29,30]. In those studies, the formation of a wetting complexion of Cr at the grain boundary results in a reduction of the grain boundary energy and thus enhanced thermal stability [30,31]. However, in systems in which segregation occurs, agglomeration of the segregated phase, which results in grain growth and reduced thermal stability has also been observed [32]. Furthermore, in previous studies of the W–Cr system, the atomic fraction of chromium was always below 15 at%, and at these compositions the formation of the W_3Cr intermetallic is also unlikely [29,30].

In this manuscript, the phase transformations occurring in the W–Cr binary system are studied using NMMs, which lead to a high density of interphases that should increase the diffusivities of W and Cr. The greater diffusivities induce mixing and result in the development of diffusion zones where new stable phases can more easily nucleate [17]. For example, the W_3Cr intermetallic, which has previously only been observed at 1350 °C, could form at lower temperatures in NMMs systems [27]. Thus, this approach opens a new alternative to explore phase formation processes in nanoscale systems.

2. Materials and Methods

For this study, Cr/W–Cr NMMs were deposited on (100) Si substrates by magnetron sputtering at 2.0 Pa using powers of 50 W and 200 W for the Cr and W sources, respectively. The composition of the films was tuned by controlling the on-time of the W source following procedures previously described [33]. The structure of the as-sputtered W–Cr NMMs is shown in the cross-sectional bright field transmission electron microscopy (TEM) image in Fig. 1(a). The overall film thickness was 2 μm and the individual layer thicknesses were 1.5 nm Cr (99.9 at% Cr) and 6.3 nm W rich (12.4 at% Cr), respectively. These thin layers increase the density of interphases and thus the local diffusivity. For example, at 550 °C, calculations made using Darken equation and diffusivity values obtained from Fisher's analysis at the interphase, show that the diffusivity of Cr in W is $D_{Cr-W} = 7.7 \times 10^{-29} m^2 s^{-1}$, while the diffusivity of Cr in W at the interphase is $D^i_{Cr-W} = 1.7 \times 10^{-28} m^2 s^{-1}$, which is more than a twofold increment [28,34–36].

The global composition of the as-sputtered sample, 65.3 at% W, 34.0 at% Cr and 0.6 at% Ar, was measured using a JSM-7001 scanning electron microscope (SEM) with an energy dispersive x-ray spectroscopy (EDS) EDAX detector. The presence of Ar is attributed to the high

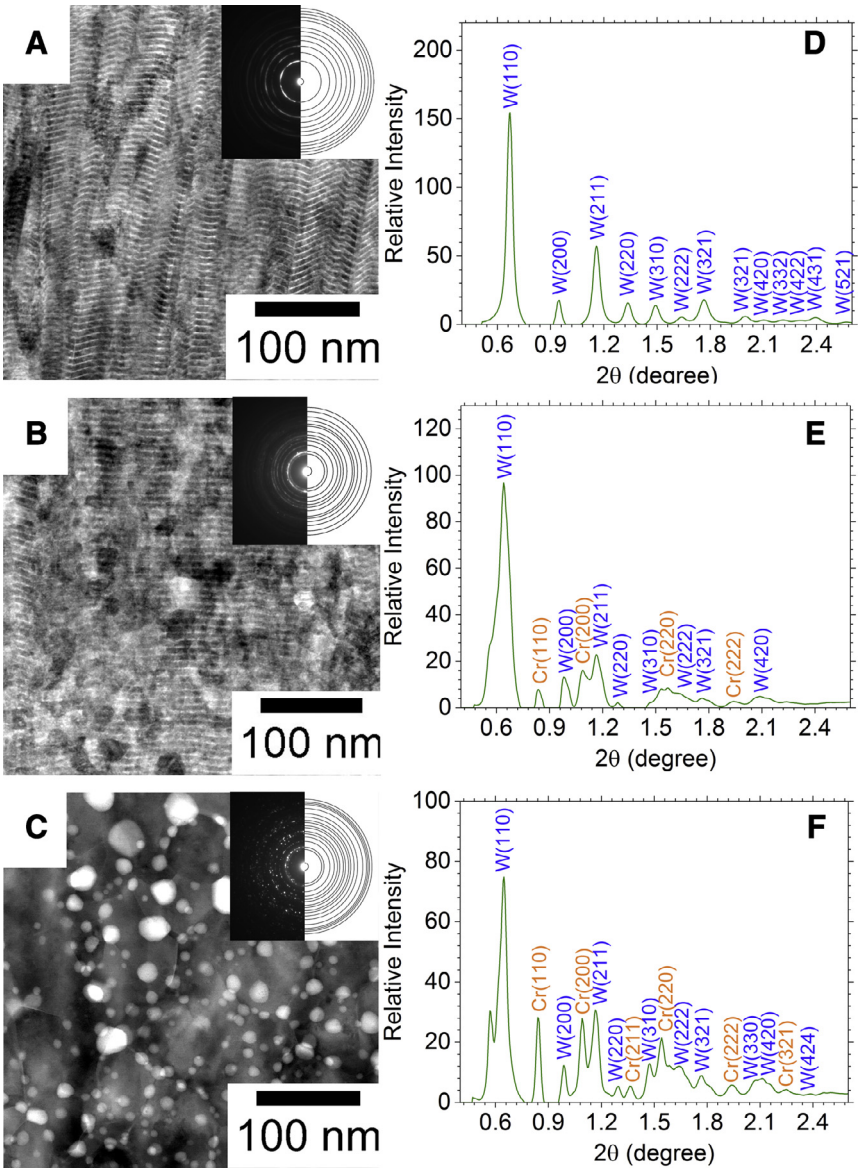

Fig. 2. Cross-sectional bright field STEM images and integrated radial intensity profile of W–Cr nanometallic multilayers heat-treated at (a)–(d) 550 °C, (b)–(e) 800 °C and (c)–(f) 1000 °C. The inset in the STEM images shows the diffraction patterns and the orientations indexed in the integrated radial intensity profiles. Note that at 550 °C the microstructure shows unaltered multilayers while at 800 °C new grains have appeared between the layers and new orientations are observed in the radial intensity profile. At 1000 °C, the sample is comprised of equiaxed grains surrounded by precipitates at the grain boundaries.

sputtering pressure used during the deposition [37]. This sample has a vertical growth direction with densely packed fibrous columnar grains characteristic of a morphology type zone 1 with grains interrupted by the pure Cr layers [38]. The average grain size of the as-sputtered sample, 9 nm, was measured following procedures described in a previous manuscript [32]. In addition, XRD scans of the as-sputtered sample, acquired using a Rigaku Ultima IV diffractometer, show a highly (110) texture. That orientation is also observed in the integrated radial intensity profile (Fig. 1(b)), which only shows α-tungsten peaks; the lack of β-tungsten peaks points to the absence of β-tungsten nucleation reported for W alloys in another sputtering study [30].

3. Results and Discussion

DSC scans of the W–Cr NMMs (Fig. 1(c)) mounted on the substrate were collected using a Si (100) substrate reference from 20 °C to 1000 °C at a rate of 10 °C per minute under a constant Ar flow of 50 ml/min in a STA 449 F5 Jupiter thermal analyzer. The DSC scans showed that recrystallization occurs between 690 °C and 830 °C with $\Delta H_{recrystallization} = -1.8$ kJ/mol, where recrystallization is then followed by grain growth which takes place between 830 °C and 990 °C with $\Delta H_{grain-growth} = -1.8$ kJ/mol. These temperature ranges suggest that above 700 °C, when recrystallization starts and the diffusivities are significantly large, the grain boundary mobility, which depends linearly on the diffusivity, should be high enough for the formation of diffusion zones where new phases could nucleate [7,35]. This is in agreement with a five order of magnitude increase in the diffusivity of Cr in W at the interphase from $D^{i}_{\mathrm{Cr-W}} = 6.3 \times 10^{-25} \mathrm{m^2 s^{-1}}$ at 700 °C to $D^{i}_{\mathrm{Cr-W}} = 3.1 \times 10^{-20}\ \mathrm{m^2 s^{-1}}$ at 1000 °C [35,36].

Guided by the DSC scans, the W–Cr NMMs were annealed at 550 °C, 800 °C and 1000 °C, for 96 h under vacuum (pressure $\approx 5 \times 10^{-4}$ Pa) inside a GSL1100X tube furnace (MTI Corporation). At the end of the heat treatments, the samples were quenched in a low vapor pressure oil (Invoil 705, Inland Vacuum Industries) without breaking vacuum. After cleaning the samples with isopropanol, TEM specimens were prepared by Focus Ion Beam (FIB) lift out using a FIB-4500 (JEOL). TEM images

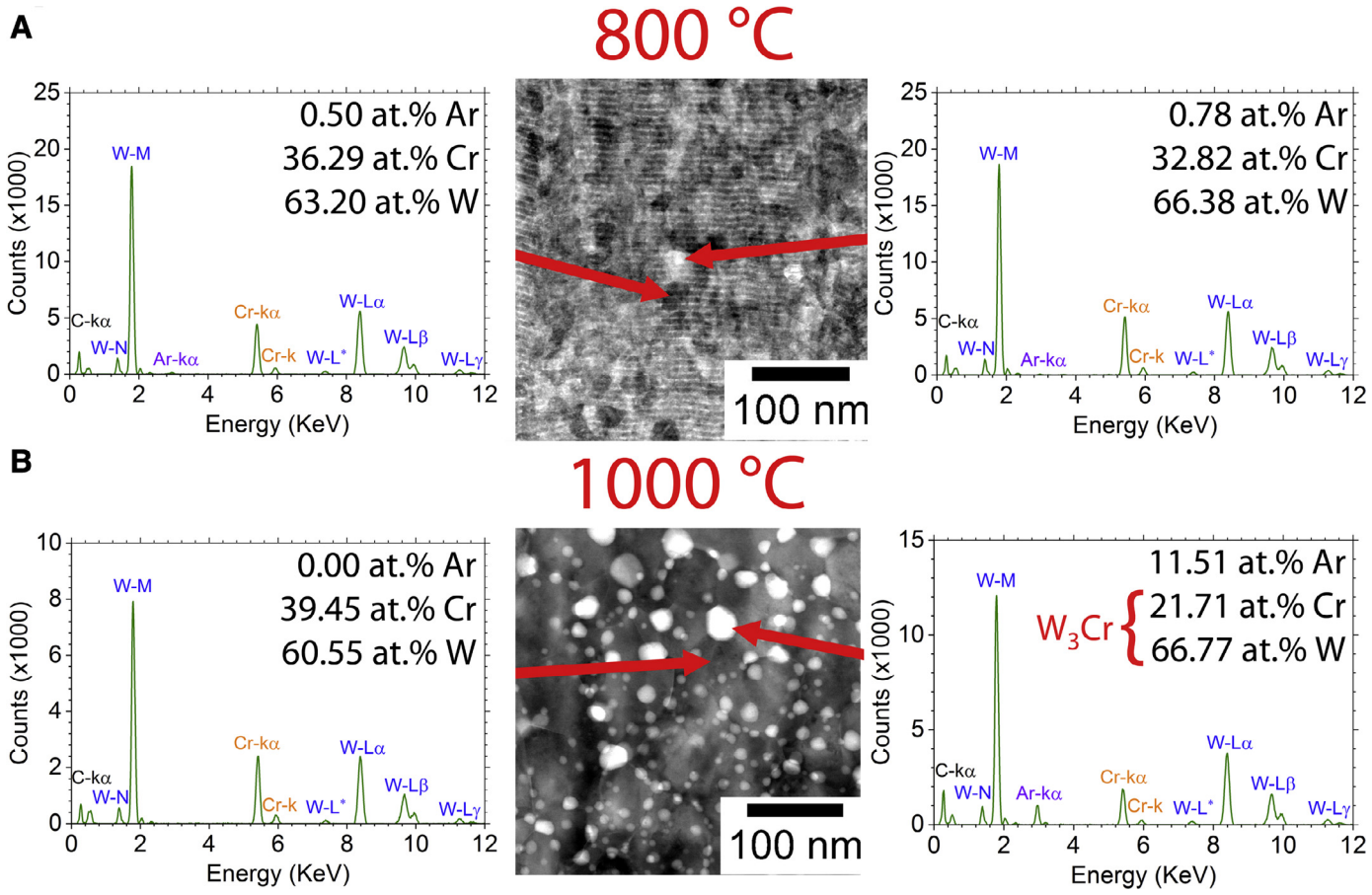

Fig. 3. EDS scans of (a) at 800 °C showing recrystallized grains and (b) at 1000 °C showing W rich grains (Dark) surrounded by W_3Cr precipitates (Bright) rich in Ar. The arrows point to the corresponding regions in the STEM images. While at 800 °C the scans highlight that the recrystallized grains have enriched in Cr, at 1000 °C, they show that the W rich grains have further enriched to 40 at% Cr.

of the sample and EDS spectra were captured on a JEM-2100F (JEOL) microscope equipped with an Oxford X-MaxN 100 EDS detector.

The DSC scans indicate that at 550 °C no microstructural transitions have occurred. Fig. 2(a) and (d) shows that at this temperature the multilayered structure is preserved without apparent changes in the grain orientation or the average grain size in comparison to the as-sputtered sample. In contrast, at 800 °C (Fig. 2(b)) the microstructure is comprised of unrecrystallized multilayers and recrystallized grains, which have an average grain size of 16 nm and show contrast due to change in orientation. Although the integrated radial intensity profile at 800 °C (Fig. 2(e)) shows new Cr peaks, no new phases were observed at this temperature. This indicates that these peaks correspond to Cr clusters forming inside the recrystallized grains.

Annealing at 1000 °C (Fig. 2(c)) resulted in grain growth and further microstructural changes; the sample is now comprised of equiaxed grains (average grain size of 78 nm) surrounded by precipitates at the grain boundaries (average grain size of 9 nm). The radial intensity profile of this sample (Fig. 2(f)) shows that in comparison to the sample annealed at 800 °C, the intensity of the Cr peaks has increased at 1000 °C, which suggests that the equiaxed grains have further enriched with Cr.

To understand the formation of precipitates observed at 1000 °C, samples heat-treated at 800 °C and 1000 °C were compared by EDS techniques. Fig. 3(a) shows that the recrystallized grains observed at 800 °C have enriched from the initial composition of the W rich layers (12.4 at% C) to ≈34.5 at% Cr, which is in agreement with the observations made from the radial intensity profile (Fig. 2(e)). Furthermore, the EDS scans show that a low fraction of deposited Ar (0.6 at% Ar) is uniformly distributed through the sample. However, at 1000 °C, the EDS scans (Fig. 3(b)) indicate that the equiaxed grains have further enriched to 39.5 at%. Cr, which corresponds to higher intensity Cr peaks in the radial intensity profiles. Inside the precipitates, the EDS scans show a 3:1 atomic ratio of W and Cr, suggesting that the precipitates could be the W_3Cr phase previously reported in the literature [27]. From here on, we will refer to the precipitates at the grain boundaries as W_3Cr precipitates. Moreover, the EDS scans indicate that at 1000 °C, Ar in the equiaxed grains has been completely depleted, while the fraction of Ar in the W_3Cr precipitates has increased to 11.5 at% Ar. The Ar depletion in the equiaxed grains can be understood by considering that above 800 °C the diffusivity of Ar increases, which facilitates the segregation of Ar to the grain boundaries [39]. Subsequently, Ar diffuses along the grain boundaries and dissolves into the W_3Cr precipitates, minimizing the Gibbs energy, which increases in the stability of the system [40,41].

To understand the formation of the W_3Cr intermetallic, Miedema's model was used to calculate the enthalpy of formation of the W_3Cr intermetallic $\Delta H^f_{W_3Cr} = 1.0$ KJ/mol, and that of a solid solution of the same composition $\Delta H^f_{Solid-solution} = 8.0$ KJ/mol. Assuming similar entropies of formation for the W_3Cr and the solid solution, these values suggest that the formation of the W_3Cr is energetically favorable [42]. In addition, the fact that the W_3Cr precipitates are localized at the grain boundaries suggests that they formed via continuous precipitation. During that precipitation process, amorphous Cr clusters appear at the grain boundaries and continue growing, due to Cr diffusing from the surrounding grains, until their composition is close to 25 at% Cr [43]. This is in agreement with the precipitation of amorphous phases (amorphization reactions) at grain boundaries and interphases observed in other multilayered sys-

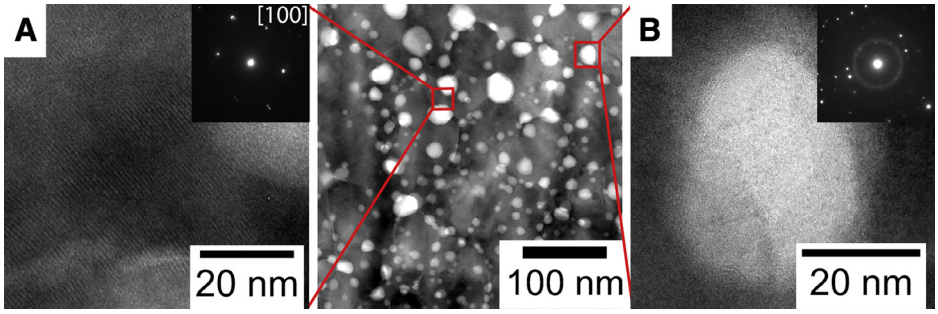

Fig. 4. High resolution bright field TEM images from the sample heat treated at 1000 °C showing (a) a W rich grain surrounded by W_3Cr precipitates and (b) an amorphous W_3Cr precipitate. The insets show the SAD patterns of the corresponding regions. (a) Displays a crystalline BCC structure, while (b) highlights an amorphous W_3Cr precipitate surrounded by a diffusion zone.

tems [17,44]. However, this result leads to the question of why W_3Cr precipitates were not observed at 800 °C even though the composition was also favorable and the diffusivities of W and Cr should have been high enough to induce the development of diffusion zones. The lack of W_3Cr nucleation at 800 °C could be due to two reasons. First, the Gibbs energy of the W_3Cr phase may be higher at 800 °C than at 1000 °C, which would make the nucleation of this intermetallic unlikely at the former temperature. However, there is lack of accurate models to compute the mixing entropy of metastable alloys that have a significant contribution from interphase effects and therefore, the Gibbs energy of the W_3Cr phase cannot be directly calculated. As an approach to understand the temperature dependence of the Gibbs energy for the W_3Cr intermetallic, the Scientific Group Thermodata Europe (SGTE) datasheet was used to calculate the Gibbs energy isotherms for the W–Cr system [45]. These isotherms showed that the Gibbs energy of this system decreases with increasing temperature and a similar trend would be expected for W_3Cr [40]. Second, considering the high melting points of W and Cr, 3422 °C and 1907 °C, respectively, it is expected that the diffusivities of both species will be slower at temperatures below half the melting point of Cr (around 850 °C). For example, at 800 °C the self-diffusivities of W and Cr are $D^*_W = 1.8 \times 10^{-31}$ m^2s^{-1} and $D^*_{Cr} = 1.6 \times 10^{-22}$ m^2s^{-1}, respectively, while at 1000 °C they are $D^*_W = 1.7 \times 10^{-27}$ m^2s^{-1} and $D^*_{Cr} = 1.1 \times 10^{-19}$ m^2s^{-1} [36]. Thus, the formation of W_3Cr nuclei may have been kinetically unlikely at or below 800 °C [15].

To understand the different phases observed at 1000 °C in more detail, high-resolution TEM images and SAD patterns of the equiaxed grains and of the W_3Cr precipitates were collected. Fig. 4(a) shows that the equiaxed grains, between the W_3Cr precipitates, have a crystalline BCC structure with a [100] zone axis [46]. Due to the small difference between the metallic radius of W and Cr (8.5% difference), these elements form a solid solution inside the equiaxed grains, which is in agreement with the Hume–Rothery rules [47]. On the other hand, Fig. 4(b) reveals that the W_3Cr precipitates are amorphous, which is confirmed by the concentric diffuse rings in the SAD pattern. In addition, there is a diffusion zone of around 5.1 nm between the precipitates and the equiaxed grains, which is crystalline at the side of the W rich grains and amorphous at the side of the W_3Cr precipitates.

The formation of amorphous W_3Cr precipitates at the grain boundaries also indicates that the activation energy barrier for nucleation is overcome by the excess Gibbs energy at grain interfaces, where the higher energy induces the nucleation of amorphous aggregates, which continue growing as the diffusivities of W and Cr increase with temperature. This process should continue above 1000 °C until the Gibbs energy of formation of crystalline W_3Cr is lower than that of the amorphous precipitates leading to crystallization. Although these events, which are highly dependent on temperature, could be affected by the presence of the Ar impurities in the system, further studies are still required. Thus far, Ar has been shown to decrease grain growth by promoting kinetic stabilization of the grain boundaries [48,49]. However, this is not related to the formation of intermetallics.

In addition to the W_3Cr precipitates, the microstructure at 1000 °C is also comprised of equiaxed grains rich in W. The composition of these grains suggests that the initial multilayered structure shifts the kinetics of nucleation towards the formation of solutions rich in W. Although there are two phases below the miscibility gap of the W–Cr system, we do not observe the Cr rich phase. This is a result of the initial W rich layers being in a stable state above 1000 °C, which lowers the Gibbs energy of W solutions and increases the energy penalty for nucleation of solutions rich in Cr [27]. Thus, the initial metastable state of the NMMs should modify the local Gibbs free energy and favor the nucleation of stable states close to that of the W rich layers, which suggests that the structure of NMMs can be tuned to favor the formation of selected stable states.

4. Conclusions

NMMs were used to control the formation of phases in the W–Cr system during annealing. Specifically, the high density of interfaces in the nanoscale multilayers increased the rate for phase transformations, such that thermal processes could be resolved at reduced temperatures. For instance, an amorphous W_3Cr intermetallic was observed at 1000 °C, a temperature much lower than that reported in previous studies. Furthermore, the multilayered structure shifted the kinetics of phase separation towards the formation of solid solutions rich in W. Overall, we propose a new alternative method to study phase transformations at the nanoscale by using NMMs to control the thermal evolution of the system.

Acknowledgments

This work was performed under the auspices of the National Science Foundation under Grant DMR-1709771 and of the Office of Naval Research under Grant N00014-12-1-0638. We acknowledge the Center for Electron Microscopy and Microanalysis at USC for the use of their SEM, FIB and TEM instruments.

Declaration of interest

The authors declare that they have no known competing financial interests or personal relationships that could have appeared to influence the work reported in this paper.

The authors declare the following financial interests/personal relationships which may be considered as potential competing interests.

References

[1] R.A. Andrievski, Review of thermal stability of nanomaterials, J. Mater. Sci. 49 (4) (2014) 1449–1460.
[2] J. Weissmuller, Nanocrystalline materials – an overview, Miner. Met. Mater. Soc. (1996).
[3] J. Weissmuller, Alloy thermodynamics in nanostructures, J. Mater. Res. 9 (1) (1994) 4–7.

[4] H. Gleiter, Nanocrystalline materials, Prog. Mater. Sci. 33 (4) (1989) 223–315.
[5] S. Simões, R. Calinas, M.T. Vieira, M.F. Vieira, P.J. Ferreira, In situ TEM study of grain growth in nanocrystalline copper thin films, Nanotechnology 21 (14) (2010) 145701.
[6] G.D. Hibbard, J.L. McCrea, G. Palumbo, K.T. Aust, U. Erb, An initial analysis of mechanisms leading to late stage abnormal grain growth in nanocrystalline Ni, Scr. Mater. 47 (2) (2002) 83–87.
[7] A. Rollett, F. Humphreys, G.S. Rohrer, M. Hatherly, Recrystallization and Related Annealing Phenomena, Elsevier, 2004.
[8] L.P. Jeurgens, Z. Wang, E.J. Mittemeijer, Thermodynamics of reactions and phase transformations at interfaces and surfaces, Int. J. Mater. Res. 100 (10) (2009) 1281–1307.
[9] P. G.B. Wilde, H. Rösner, J. Weissmüller, Phase Equilibria of Nanoscale Metals and Alloys, D. M. Herlach, 2009.
[10] V.I. Levitas, M. Javanbakht, Phase transformations in nanograin materials under high pressure and plastic shear: nanoscale mechanisms, Nanoscale 6 (1) (2014) 162–166.
[11] S. Ruffell, J.E. Bradby, J.S. Williams, D. Munoz-Paniagua, S. Tadayyon, L.L. Coatsworth, P.R. Norton, Nanoindentation-induced phase transformations in silicon at elevated temperatures, Nanotechnology 20 (13) (2009) 135603.
[12] M. Tsuchiya, A.M. Minor, S. Ramanathan, Size-dependent phase transformations in nanoscale pure and Y-doped zirconia thin films, Philos. Mag. 87 (36) (2007) 5673–5684.
[13] H.J. Lee, K.W. Kwon, C. Ryu, R. Sinclair, Thermal stability of a Cu/Ta multilayer: an intriguing interfacial reaction, Acta Mater. 47 (15–16) (1999) 3965–3975.
[14] V.I. Levitas, M. Javanbakht, Interaction of phase transformations and plasticity at the nanoscale: phase field approach, Mater. Today: Proc. 2 (2015) S493–S498.
[15] J.W. Christian, The Theory of Transformations in Metals and Alloys, Newnes, 2002.
[16] M. Bobeth, A. Ullrich, W. Pompe, Destratification mechanisms in coherent multilayers, J. Metastab. Nanocryst. Mater. Trans. Tech. Publ. (2004) 153.
[17] A.M. Gusak, T. Zaporozhets, Y.O. Lyashenko, S. Kornienko, M. Pasichnyy, A. Shirinyan, Diffusion-controlled Solid State Reactions: In Alloys, Thin-Films, and Nanosystems, John Wiley & Sons, 2010.
[18] H.-J. Lee, K.-W. Kwon, C. Ryu, R. Sinclair, Thermal stability of a Cu/Ta multilayer: an intriguing interfacial reaction, Acta Mater. 47 (15–16) (1999) 3965–3975.
[19] M.Z. Wei, Z.H. Cao, J. Shi, G.J. Pan, L.J. Xu, X.K. Meng, Evolution of interfacial structures and creep behavior of Cu/Ta multilayers at room temperature, Mater. Sci. Eng.: A 646 (2015) 163–168.
[20] A.M. Gusak, F. Hodaj, A.O. Bogatyrev, Kinetics of nucleation in the concentration gradient, J. Phys.: Condens. Matter 13 (12) (2001) 2767.
[21] D. Kashchiev, Nucleation, Elsevier, 2000.
[22] T. Chookajorn, H.A. Murdoch, C.A. Schuh, Design of stable nanocrystalline alloys, Science 337 (6097) (2012) 951–954.
[23] H.A. Murdoch, C.A. Schuh, Stability of binary nanocrystalline alloys against grain growth and phase separation, Acta Mater. 61 (6) (2013) 2121–2132.
[24] K.A. Darling, M.A. Tschopp, B.K. VanLeeuwen, M.A. Atwater, Z.K. Liu, Mitigating grain growth in binary nanocrystalline alloys through solute selection based on thermodynamic stability maps, Comput. Mater. Sci. 84 (2014) 255–266.
[25] M.A. Atwater, K.A. Darling, A visual library of stability in binary metallic systems: the stabilization of nanocrystalline grain size by solute addition: part 1, DTIC Document, 2012.
[26] H.A. Murdoch, C.A. Schuh, Estimation of grain boundary segregation enthalpy and its role in stable nanocrystalline alloy design, J. Mater. Res. 28 (16) (2013) 2154–2163.
[27] S.V.N. Naidu, A.M. Sriramamurthy, P.R. Rao, The Cr–W (Chromium–Tungsten) system, Bull. Alloy Phase Diagr. 5 (3) (1984) 289.
[28] H. Mehrer, Diffusion in Solids: Fundamentals, Methods, Materials, Diffusion-Controlled Processes, Springer Berlin Heidelberg, 2007.
[29] T. Chookajorn, M. Park, C.A. Schuh, Duplex nanocrystalline alloys: entropic nanostructure stabilization and a case study on W–Cr, J. Mater. Res. 30 (2) (2015) 151–163.
[30] O.K. Donaldson, K. Hattar, T. Kaub, G.B. Thompson, J.R. Trelewicz, Solute stabilization of nanocrystalline tungsten against abnormal grain growth, J. Mater. Res. 33 (1) (2017) 68–80.
[31] P.R. Cantwell, M. Tang, S.J. Dillon, J. Luo, G.S. Rohrer, M.P. Harmer, Grain boundary complexions, Acta Mater. 62 (2014) 1–48.
[32] J.S. Riano, A.M. Hodge, Exploring the microstructural evolution of Hf-Ti: From nanometallic multilayers to nanostructures, Scr. Mater. 142 (2018) 55–60.
[33] M.N. Polyakov, T. Chookajorn, M. Mecklenburg, C.A. Schuh, A.M. Hodge, Sputtered Hf–Ti nanostructures: a segregation and high-temperature stability study, Acta Mater. 108 (2016) 8–16.
[34] K.-N. Tu, A.M. Gusak, Kinetics in Nanoscale Materials, John Wiley & Sons, 2014.
[35] I. Kaur, Y. Mishin, W. Gust, Fundamentals of Grain and Interphase Boundary Diffusion, Wiley, 1995.
[36] J.N. Mundy, S.J. Rothman, N.Q. Lam, H.A. Hoff, L.J. Nowicki, Self-diffusion in tungsten, Phys. Rev. B 18 (12) (1978) 6566–6575.
[37] W.W. Lee, D. Oblas, Argon concentration in tungsten films deposited by dc sputtering, J. Vac. Sci. Technol. 7 (1) (1970) 129–133.
[38] J.A. Thornton, Influence of apparatus geometry and deposition conditions on the structure and topography of thick sputtered coatings, J. Vac. Sci. Technol. 11 (4) (1974) 666–670.
[39] E.H.C. Parker, H.R. Glyde, B.L. Smith, Self-diffusion in solid argon, Phys. Rev. 176 (3) (1968) 1107–1110.
[40] M. Hillert, Phase Equilibria, Phase Diagrams and Phase Transformations: Their Thermodynamic Basis, Cambridge University Press, 2007.
[41] S.R. De Groot, P. Mazur, Non-equilibrium Thermodynamics, Courier Corporation, 2013.
[42] H. Bakker, Enthalpies in Alloys, Miedema's Semi-Empirical Model, Trans. Tech. Publications, 1998.
[43] D. Kashchiev, On the relation between nucleation work, nucleus size, and nucleation rate, J. Chem. Phys. 76 (10) (1982) 5098–5102.
[44] R. Benedictus, A. Böttger, E.J. Mittemeijer, Thermodynamic model for solid-state amorphization in binary systems at interfaces and grain boundaries, Phys. Rev. B 54 (13) (1996) 9109–9125.
[45] P. Franke, D. Neuschütz, Binary Systems. Part 2: Elements and Binary Systems from B–C to Cr–Zr•Cr–Mg: Datasheet from Landolt-Börnstein – Group IV Physical Chemistry Volume 19B2, Springer-Verlag, Berlin Heidelberg, 2004.
[46] B. Fultz, J.M. Howe, Transmission Electron Microscopy and Diffractometry of Materials, Springer Science & Business Media, 2012.
[47] B. Fultz, Phase Transitions in Materials, Cambridge University Press, 2014.
[48] B. Huang, R.J. Perez, E.J. Lavernia, Grain growth of nanocrystalline Fe–Al alloys produced by cryomilling in liquid argon and nitrogen, Mater. Sci. Eng.: A 255 (1–2) (1998) 124–132.
[49] C.J. Marvel, D. Yin, P.R. Cantwell, M.P. Harmer, The influence of oxygen contamination on the thermal stability and hardness of nanocrystalline Ni–W alloys, Mater. Sci. Eng.: A 664 (2016) 49–57.